Radar Noise Reduction Based on Binary Integration

Daniel Lühr, *Member, IEEE*, and Martin Adams, *Senior Member, IEEE*

***Abstract*— Short range radars can provide robust information about their surroundings under atmospheric disturbances, such as dust, rain, and snow, conditions under which most other sensing technologies fail. However, this information is corrupted by received power noise, resulting in false alarms, missed detections, and range/bearing uncertainty. The reduction of radar image noise, for human interpretation, as well as the optimal, automatic detection of objects, has been a focus of radar processing algorithms for many years. This paper combines the qualities of the well established binary integration detection method, which manipulates multiple images to improve detection within a static scene, and the noise reduction method of power spectral subtraction. The binary integration method is able to process multiple radar images to provide probability of detection estimates, which accompany each power value received by the radar. The spectral subtraction method then utilizes these probabilities of detection to form an adaptive estimate of the received noise power. This noise power is subtracted from the received power signals, to yield reduced noise radar images. These are compared with state-of-the-art noise reduction methods based on the Wiener filter and wavelet denoising techniques. The presented method exhibits a lower computational complexity than the benchmark approaches and achieves a higher reduction in the noise level. All of the methods are applied to real radar data obtained from a 94-GHz millimetre wave FMCW 2D scanning radar and to synthetic aperture radar data obtained from a publicly available data set.**

***Index Terms*— Binary integration, CFAR, data integration, image denoising, millimeter wave radar, noise reduction, noise subtraction, radar detection, radar imaging, wavelet denoising, Wiener filter, SAR.**

I. Introduction

LANDMARK identification concerns the detection of signals from noisy measurement data. When time is available to obtain multiple images from a static scene at the same location, it is possible to exploit the correlation in the sequence of images to reduce noise, and consequently improve detection. A noise reduction method applied to radar data using these concepts is presented in this work.

Several methods have been developed in the field of image processing to reduce noise in both stationary and dynamic image sequences in applications as diverse as object tracking surveillance, autonomous navigation, motion analysis, and astronomical and medical imaging [1]. A sequence of 2D images is represented by a 3D volume where the third dimension corresponds to the temporal dimension or the sequence index. Many of the methods to process such 3D signals have been developed by generalising well known 2D filtering techniques by extending the support of a filter in the temporal domain. The classical Wiener filter [2], extended to a 3D form, is an example of such an approach. The Wiener filter is a linear time-invariant estimator which adopts a *Minimum mean square error* (MSE) statistical approach. Adaptive noise cancelling, developed as a variation of the original Wiener optimal filtering theory, was presented in [3]. The adaptive noise cancelling application uses a reference signal correlated with the noise to obtain a noise estimate. This estimate is then subtracted from the noisy signal. An application of Wiener filtering to 3D medical imaging data [4] extends the classical Wiener implementation by estimating the filter parameters using a sequence of observations based on the calculation of local statistics (calculated in a small window around the point of interest). In radar applications, a 2D Wiener filter, also using local statistics, has been used to reduce noise in weather radar data [5].

Work by Donoho and Johnstone [6]–[8] introduced the denoising capabilities of the Wavelet transform. The basic method is *Denoising by Thresholding* [9]. It is analogous to frequency domain filtering based on the Fourier transform. The wavelet time-frequency approach however, attempts to reduce noise by preserving a number of coefficients associated with components with high information energy, and discarding the rest. It is assumed that noise (often considered to be additive Gaussian) is spread homogeneously among all signal frequency components. Thus by discarding the coefficients of the components not highly correlated with the signal, a significant amount of noise is eliminated. Coefficients with a magnitude higher than the threshold are considered to hold mostly signal information, and those lower than the threshold are considered to carry mainly noise energy. In radar applications several articles have demonstrated the use of wavelets to reduce noise. Chen [10] proposed a recursive thresholding method for radar image denoising, while Aly demonstrated the use of wavelet packet transforms and higher order statistics to detect and localise RF radar pulses in noisy environments [11]. In general, most noise reduction algorithms (both 'classical' and wavelet-based) assume the noise to be additive Gaussian [1], [9], which is useful for a broad range of applications. However, in radar imaging, the Gaussian noise assumption is often unrealistic. Another critical aspect

Manuscript received June 7, 2014; accepted August 10, 2014. Date of publication August 26, 2014; date of current version November 20, 2014. This work was supported in part by Conicyt Fondecyt Project 1110579, in part by Conicyt-DAAD PCCI-2012009, and in part by AMTC, Universidad de Chile. The associate editor coordinating the review of this paper and approving it for publication was Dr. Lorenzo Lo Monte.

D. Lühr is with the Department of Electrical Engineering, University of Chile, Santiago, Chile (e-mail: dluhr@ieee.org).

M. Adams is with the Department of Electrical Engineering, University of Chile, Santiago, Chile, and also with the Advanced Mining Technology Center, University of Chile, Santiago 1058, Chile (e-mail: martin@ing.uchile.cl).

Color versions of one or more of the figures in this paper are available online at http://ieeexplore.ieee.org.

Digital Object Identifier 10.1109/JSEN.2014.2352295

of wavelet denoising is the appropriate threshold selection. An adaptive threshold method was introduced by Chen [12], which adapts the threshold to the coefficients' statistics, relaxing the Gaussian assumption of most wavelet based methods. Another adaptive method, presented by Jin [13] uses abrupt changes in the signal to adapt weights to calculate local means and variances. This approach is reported to reduce the ripple-like artifacts usually found around edges when using wavelet denoising techniques.

In this work a different approach for radar image denoising is introduced and compared to the classical Wiener filter and to the more recent wavelet based denoising approaches. The proposed method's implementation presents a lower computational complexity than both the 3D Wiener filter and the 3D wavelet approaches. The method further reduces the mean noise value when compared with the other two methods. It uses statistical information provided by the Binary integration detector to identify parts of the received signal corresponding to noise. It uses those parts to obtain an estimate of the noise power spectrum by recursive averaging. This noise estimate is then used for power spectral subtraction [14] (or noise subtraction) to reduce noise. In particular, Binary Integration (BI) combines the output of several single-observation detectors to improve the detection probability, while maintaining the desired, acceptable false alarm rate. The single-observation detector used is a member of the Constant False Alarm Rate (CFAR) family of stochastic detectors, widely used in radar [15].

The following section summarises classical radar detection and demonstrates its application to scanning radar images. Section III presents the three different noise reduction techniques, which will be applied to scanned radar data for comparison purposes. Section IV then explains the implementation details of the methods and analyses the implementation complexity for the three different approaches. Finally, results using millimetre wave (MMW) radar data in an outdoor environment and an open *Synthetic Aperture Radar* SAR data set are also presented in Section V.

II. Radar Detection

Targets of interest in radar data are usually embedded in noise and clutter. Thus, landmark detection is necessary to identify landmark signals from the noisy power measurement data. In this work, statistical information provided by detection methods is used to obtain a noise estimate from a sequence of radar measurements of the same scene. The noise estimate is then used in a noise subtraction method to obtain a reduced noise version of the radar power measurement data.

This section briefly describes the detection methods used, their main equations and parameters and their most important aspects.

Adaptive, stochastic, landmark detection techniques offer principled methods of detection based on a predefined acceptable probability of false alarm and quantifiable probabilities of detection. The Constant False Alarm Rate (CFAR) concept refers to a family of adaptive algorithms widely used in radar to detect target returns against a background of noise, clutter and interference.

In most radar signal processing literature to date, a Cell Averaging (CA) CFAR detector is the preferred method of target detection [16]–[18]. A CA-CFAR processor is used on the experimental data presented in Section V-B.

[19] shows that the detection probability $P_D^{\text{CA-CFAR}}(q)$ of a Rayleigh fluctuating target, embedded in exponential noise or clutter, can be determined from the CA-CFAR parameters

$$P_D^{\text{CA-CFAR}}(q) = \left[1 + \frac{\tau^{\text{CA-CFAR}}}{W_f}\left(\frac{1}{1+\widehat{\eta}^{\text{SNP}}(q)}\right)\right]^{-W_f} \quad (1)$$

where W_f is the size of the CFAR window and $\tau^{\text{CA-CFAR}}$ is defined as

$$\tau^{\text{CA-CFAR}} = W_f\left(\left(P_{fa}^{\text{CA-CFAR}}\right)^{\frac{-1}{W_f}} - 1\right) \quad (2)$$

and $\widehat{\eta}^{\text{SNP}}(q)$ is the estimated received SNP calculated as

$$\widehat{\eta}^{\text{SNP}}(q) = \frac{S_{\text{lin}}^{\text{radar}}(q)}{T(S_{\text{lin}}^{\text{radar}}(q))} \quad (3)$$

where $S_{\text{lin}}^{\text{radar}}(q)$ is the linearised received power from the radar in the q^{th} (bearing-range) bin, and $T(S_{\text{lin}}^{\text{radar}}(q))$ is the CFAR test statistic, which in the case of CA-CFAR, corresponds to the sample mean of the neighbouring cell's power values in the CFAR window. The adaptive threshold is then defined as

$$S_{\text{lin}}^{\text{CA-CFAR}}(q) = \tau^{\text{CA-CFAR}} \cdot T(S_{\text{lin}}^{\text{radar}}(q)). \quad (4)$$

Several other CFAR methods have been developed and current research focuses in CFAR methods with adaptive parameters [20]. In particular, the Ordered Statistic (OS) CFAR has been reported to perform well for large targets (with respect to the spatial resolution) and in SAR images, due to their noise and clutter being usually modelled by Weibull or K distributions, and the higher effect of multiplicative speckle noise present in such images. The OS-CFAR method is used on the SAR data set presented in Section V-C.

In the OS-CFAR method the test statistic $T(S_{\text{lin}}^{\text{radar}}(q))$ is obtained by choosing the k^{th} value from the ordered set of power values in the CFAR window

$$S_{\text{lin}}^{(1)} \le S_{\text{lin}}^{(2)} \le \ldots \le S_{\text{lin}}^{(k)} \le \ldots \le S_{\text{lin}}^{(W_f-1)} \le S_{\text{lin}}^{(W_f)} \quad (5)$$

a value of $k = \frac{3W_f}{4}$ has been suggested in [21] to represent a good estimate for typical radar applications. The parameter $\tau^{\text{OS-CFAR}}$ needs to be calculated numerically from

$$P_{fa}^{\text{OS-CFAR}} = \prod_{i=0}^{k-1} \frac{W_f - i}{W_f - i + \tau^{\text{OS-CFAR}}} \quad (6)$$

where $P_{fa}^{\text{OS-CFAR}}$ is the chosen acceptable OS-CFAR probability of false alarm. The probability of detection, $P_D^{\text{OS-CFAR}}(q)$, is obtained from

$$P_D^{\text{OS-CFAR}}(q) = \prod_{i=0}^{k-1} \frac{W_f - i}{W_f - i + \frac{\tau^{\text{OS-CFAR}}}{1+\widehat{\eta}^{\text{SNP}}(q)}} \quad (7)$$

Unfortunately, the noise and target distribution assumptions in CFAR are often violated, yielding higher false alarm

and missed detection rates than those theoretically derived. To reduce this problem, and if time is available to acquire multiple scans of a fixed environment, it makes sense to exploit the high target correlation between scans to further reduce the uncertainty in the existence of objects and reduce the noise. Techniques which implement this concept are generally referred to as integration methods. A simple but effective method widely used in the radar community is the Binary Integration (BI) Method [19].

When integrating L scans, the probability of detection yielded by this method is

$$P_D^{\mathrm{BI}} = \sum_{j=M^{\mathrm{BI}}}^{L} \frac{L!}{j!(L-j)!} \left(P_D^{\text{CA-CFAR}}\right)^j \left(1 - P_D^{\text{CA-CFAR}}\right)^{L-j} \tag{8}$$

where $P_D^{\text{CA-CFAR}}$ is the probability of detection in a *single scan*, and $M^{\mathrm{BI}} < L$ is the optimal BI parameter for a given L. Likewise, if $P_{fa}^{\text{CA-CFAR}}$ is the probability of false alarm in a single scan, then the probability of false alarm for the binary integration method is

$$P_{fa}^{\mathrm{BI}} = \sum_{j=M^{\mathrm{BI}}}^{L} \frac{L!}{j!(L-j)!} \left(P_{fa}^{\text{CA-CFAR}}\right)^j \left(1 - P_{fa}^{\text{CA-CFAR}}\right)^{L-j} \tag{9}$$

BI offers a robust technique to identify which parts of signal are noise. The detection probability obtained by means of the BI method will be used as a target existence probability estimate in the radar noise reduction method presented in section III-C.

III. Noise Reduction Methods

In this section three different noise reduction approaches are described. The first state of the art method is based on a version of the linear Wiener filter which uses estimates of the local means and variances in order to estimate the noise characteristics. The second, more recent, non-linear method, is a wavelet denoising approach. The final method, proposed in this article, is based on spectral noise subtraction. This method, is capable of preserving non-linear features.[1]

A. Wiener Filter

This method of noise reduction corresponds to the application of a discrete-time minimum-mean-square-error filter. Such a filter is known as a Wiener-Kolmogorov filter or Wiener filter for short [22], [23].

Wiener filters assume additive noise and that the signals are stationary, linear stochastic processes. Because radar images, as well as natural images, consist of smooth areas, textures and edges, they are not *globally* stationary, but can be treated as *locally* stationary. This led to the derivation of the Lee filter [24], which has been extensively used in video denoising, where it has proved to be successful in terms of noise removal and preserving some important image features (e.g. edges) [13]. The Lee filter assumes that all samples within a local window are from the same structure (local stationarity). This assumption is invalid when sharp edges are encountered within the window, therefore the mean is blurred and the variance increases near the edges, which results in a degraded image near those regions.

B. Wavelet Denoising

Some of the limitations of the Wiener filter, particularly its inability of preserving non-linear features in the data, can be overcome by using non-linear filters. However, in general, finding the parameters for a non-linear filter is a complex task. Since the introduction of the wavelet denoising methods by Donoho and Johnstone [6]–[8] a powerful, yet simple to implement non-linear filter for noise reduction has become available and is widely used in practical implementations.

The particular thresholding function used in this work is the universal threshold proposed by Donoho and Johnstone [25], [26] with the soft-thresholding method proposed in [6].

This method generates an estimated signal with a smaller amplitude than the original one, but it retains the regularity[2] of the signal.

C. Spectral Noise Subtraction

Noise subtraction methods were originally devised for noise reduction in noisy speech signals [27]. In the case of radar data, the binary integrator's probability of detection can be used to identify sections which have low probability of having any target information and therefore they can be used to estimate the noise magnitude.

The noise power estimate $\widehat{\Sigma}_n(l)$, when the l^{th} observation has been received, can be calculated as in Equation (10), which corresponds to a recursive smoother using a fixed parameter α_d, and the binary integration probability of detection from Equation (8).

$$\begin{aligned}\widehat{\Sigma}_n(l) = &\left(\alpha_d \widehat{\Sigma}_n(l-1) + (1-\alpha_d) S_{\mathrm{lin}}^{\mathrm{radar}}(l)\right)\left(1 - P_D^{\mathrm{BI}}(l)\right) \\ &+ \widehat{\Sigma}_n(l-1) \times P_D^{\mathrm{BI}}(l)\end{aligned} \tag{10}$$

where l corresponds to the observation number. The first term on the right of Equation (10) represents the smoothed (averaged) noise power, weighted by $\left(1 - P_D^{\mathrm{BI}}(l)\right)$ during *target absence* sections of the signal, while the second term shows that the previous estimate is preserved and not updated if there is a high probability of *target presence* $\left(P_D^{\mathrm{BI}}(l) \to 1\right)$. Introducing

$$\tilde{\alpha}_d(l) = \alpha_d + (1-\alpha_d) P_D^{\mathrm{BI}}(l) \tag{11}$$

Equation (10) can be rewritten as

$$\widehat{\Sigma}_n(l) = \tilde{\alpha}_d(l) \widehat{\Sigma}_n(l-1) + \left[1 - \tilde{\alpha}_d(l)\right] S_{\mathrm{lin}}^{\mathrm{radar}}(l) \tag{12}$$

In Equation (11), $\tilde{\alpha}_d(l)$ is a time varying smoothing parameter. Hence the noise spectrum can be estimated using past

[1] non-linear features refer, in general, to sharp edges or discontinuities within a signal. E.g., in radar data, the sudden change in received power caused by the presence of a target.

[2] regularity corresponds to areas in which the signal is continuous, while discontinuities correspond to irregular points.

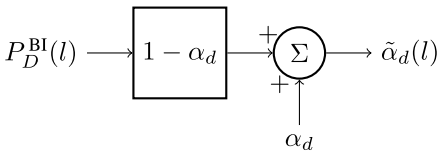

Fig. 1. Block diagram summarizing the time varying parameter $\tilde{\alpha}_d$.

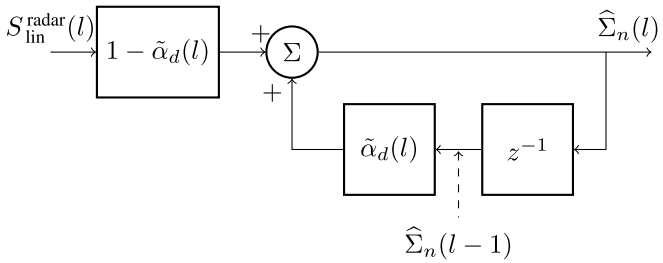

Fig. 2. Binary integration noise reduction block diagram.

spectral received power values, together with a smoothing parameter which itself varies according to the BI probability of detection $P_D^{\mathrm{BI}}(l)$. The adaptive noise estimator is summarised in the block diagrams of Figures 1 and 2.

The noise power estimate $\widehat{\Sigma}_n(l)$ can be used to obtain a *Binary Integration Noise Reduction* (BINR) power estimate $\hat{S}_{\mathrm{lin}}^{\mathrm{BINR}}(l)$ using the method of power spectral subtraction [14]. In the basic spectral subtraction algorithm, the average noise power, $\widehat{\Sigma}_n(l)$ is subtracted from the noisy range spectrum. In [28], a method which further reduces background noise for SNPs between -5 and 20 dB was devised based on subtracting an over-estimate of the noise power and preventing the resultant spectral components from reaching below a preset minimum level, termed the "spectral floor". This method leads to a reduced noise power estimate $\hat{S}_{\mathrm{lin}}^{\mathrm{BINR}}(l)$ given by

$$\widehat{S}_{\mathrm{lin}}^{\mathrm{BINR}}(l) = \begin{cases} S_{\mathrm{lin}}^{\mathrm{radar}}(l) - c\,\widehat{\Sigma}_n(l) & \text{if } S_{\mathrm{lin}}^{\mathrm{radar}}(l) > c\,\widehat{\Sigma}_n(l) \\ d \times \widehat{\Sigma}_n(l) & \text{otherwise} \end{cases} \tag{13}$$

where c is an over-subtraction factor ($c \geq 1$) and d is the spectral floor parameter ($0 < d < 1$). A value of c which is larger than 1 represents the fact that it is necessary to subtract more than the expected value of the noise (which is a smoothed estimate) to make sure that most of the noise peaks are removed. The spectral floor parameter d, when greater than zero, ensures that the remnants of the noise peaks are masked by neighbouring spectral components of comparable magnitude. This results in a reduction of broadband noise, when compared with the original power spectral subtraction method. [28] further demonstrated the advantages of an adaptive over-subtraction factor c, which varies between frames of recorded spectra, as a function of the estimated signal.

IV. Implementation and Computational Complexity

This section discusses the implementation and computational complexity, as a function of the data size, of all three noise reduction methods. All the algorithms were implemented using the SciPy signal processing toolbox [29]. The same received radar power signal S is used as the input for all the methods. The signal includes additive noise. It is a 3D array formed by stacking L radar scans. Each radar scan $S(l)$ corresponds to a B-scope of size $N_p = N_r \times N_b$ cells (pixels), where N_r represents the number of range bins (rows) while N_b the number of bearing bins (columns). The first dimension in the 3D array represents range (r), the second represents bearing (b) and the third represents the scan number (l). The sequence of L power values for a particular range and bearing is denoted as $S_{r,b}$ while an individual voxel is referred to as $S_{r,b,l}$. The total number of voxels in S is $N_v = N_b \times N_r \times L$. The complexity analysis will be carried out in terms of N_p and L ($N_v = N_p \times L$), to separate the effects of the radar image size from those related to the number of observations.

A. Wiener Filter

The Wiener filter noise reduction technique used in this work requires a support volume, in order to calculate the local means and variances. For a given voxel, the cells contained in the support volume around it will be used to calculate the local statistics. Let $(2K_r+1)$, $(2K_b+1)$, $(2K_l+1)$ be the dimensions of this volume in the range (rows), bearing (columns) and observation (depth) dimensions. K_r and K_b are related to the expected range and bearing size of targets. If these parameters are set too high the local mean and variance of a target voxel will incorporate not only target values but also undesired noise values. On the other hand, if they are to small, the local mean and variance estimates would be degraded. $2K_l + 1 = L$ has been chosen for the window to incorporate information from all observations at each value in the temporal (l) dimension. This algorithm exhibits a complexity of the order $\mathcal{O}(N_p \times L^2)$.

B. Wavelet Denoising

The 3D wavelet denoising method has been separated into two sequential wavelet denoising problems. The first carries out scan by scan 2D spatial wavelet denoising, while the second executes 1D time domain wavelet denoising for each range-bearing cell sequence. General wavelet methods have a complexity of order $\mathcal{O}(N \log N)$, where N corresponds to the data size (total number of pixels for 2D, or signal length for the 1D case). Therefore, the first part is of the order $\mathcal{O}(L \times N_p \log N_p)$ while the second part presents a complexity of the order $\mathcal{O}(N_p \times L \log L)$. Hence the total complexity of the wavelet method is of the order $\mathcal{O}(L \times N_p \log N_p + N_p \times L \log L)$ which reduces to $\mathcal{O}\big((N_p \times L)\log(N_p \times L)\big)$.

C. Binary Integration Noise Reduction

The optimum parameters required for Binary Integration, $M_{\mathrm{opt}}^{\mathrm{BI}}$ and $P_{fa}^{\mathrm{CA\text{-}CFAR}}$, can be calculated off-line and they are not included in the algorithm, but given as inputs. Also, the BI probability of detection, which is dependent on $M_{\mathrm{opt}}^{\mathrm{BI}}$ and L, can also be defined offline, and the corresponding polynomial in $P_{D_{r,b,l}}^{\mathrm{CA\text{-}CFAR}}$ is therefore, pre-calculated. The combination of the CA-CFAR, BI and noise subtraction parts of the algorithm yields a complexity of the order $\mathcal{O}(N_p \times L)$.

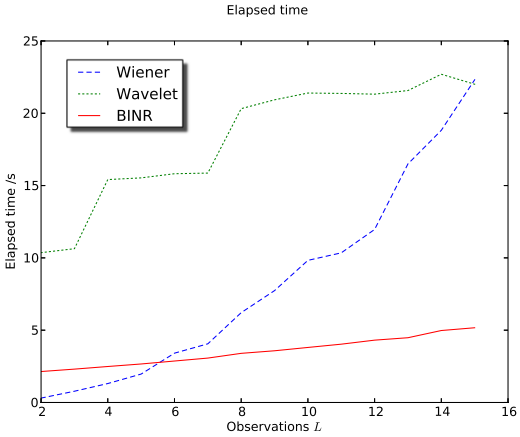

Fig. 3. Elapsed computational time measurement.

Fig. 4. Park environment where radar data was captured (obtained from Google Earth).

In summary, with respect to observations L, the Wiener filter algorithm has the highest complexity (quadratic), followed by the linearithmic[3] complexity of the Wavelet approach, while the binary integration noise reduction's linear complexity makes it the least complex. On the other hand, the Wiener filter and the binary integration noise reduction are the least complex (linear time) with respect to the data size N_v.

V. Results

All of the noise reduction methods have been tested with real data obtained in a local park environment and with an open SAR image data set. The results show reduced noise radar power in PPI representation, as well as, the average noise level versus observation number. In order to demonstrate the usefulness of each reduced noise data set, the CFAR detection method is finally applied to each set. CA-CFAR is used in the park data set due to its compliance to the detector requirements as described in Section II, while OS-CFAR is used in the SAR data set, which has been proven to be more effective with this kind of data [34]. The reduced noise CFAR output is then compared to the CFAR detector's result on the original noisy data. The computational times of the algorithms are also compared.

A. Computational Time

The computational time used by the different algorithms, plotted against observation number L, is shown in Figure 3. The results are consistent with the analysis presented in section IV. The Wiener filter's complexity grows approximately quadratically with L, while the wavelet exhibits linearithmic complexity. A linear time complexity is achieved by the BINR method.

B. Experimental Data

An experimental radar data set, captured[4] in a public park in Santiago, is used to test the noise reduction schemes.

[3]A *linearithmic* function is of the form $n \log n$. An algorithm with a time complexity of the order $\mathcal{O}(n \log n)$ is said to run in *linearithmic* time.

[4]using an Acumine 94 GHz, scanning radar [31].

TABLE I
Optimal M^{BI} Parameter for Different Number of Observations L

L	2	5	10	15	20
M^{BI}	1	2	4	5	7

1) Noise Reduction: Noise values in real radar data do not conform to perfect Gaussian or exponential distributions, as assumed by the noise reduction methods, which impairs their performance. An analysis of the noise reduction methods considering the park environment now follows. Although the methods were applied to the B-Scope radar data (range vs. bearing), the results are shown in *plan position indicator* (PPI) form for clearer visualisation. The test environment is shown in Figure 4. The area corresponds to a main paved track approximately 65 m wide. On the sides of the track there are lamp posts and some trees. There are also fences and concrete walls. The radar was located on the track.

The CA-CFAR window size was 9 bins in the bearing direction and 7 bins in the range direction. The guard cells window size was 5 in the bearing dimension and 3 bins in the range direction. These parameters were found suitable, in preliminary experiments, for detecting the lamp posts and trees surrounding the radar, by considering the power spread these features produce in the acquired data.

The BI false alarm rate used was 1×10^{-6}. The optimal M^{BI} has been previously obtained for different L values. Some of the values are listed in Table I. The results presented correspond to $L = 20$ observations. For the noise subtraction algorithm, the chosen parameters were $\alpha_d = 0.9$, $c = 50.0$ and $d = 0.1$. A high α_d ensures that the previous value of the noise estimate has more weight than the new observation which is desirable given the high noise levels present in radar data. Parameter c, controlling over-subtraction, was selected by testing different values between 10 and 100. Similarly, the spectral floor parameter d was tested for different values between 0.05 to 0.5, with the chosen value yielding good results in the reduction of the broadband noise.

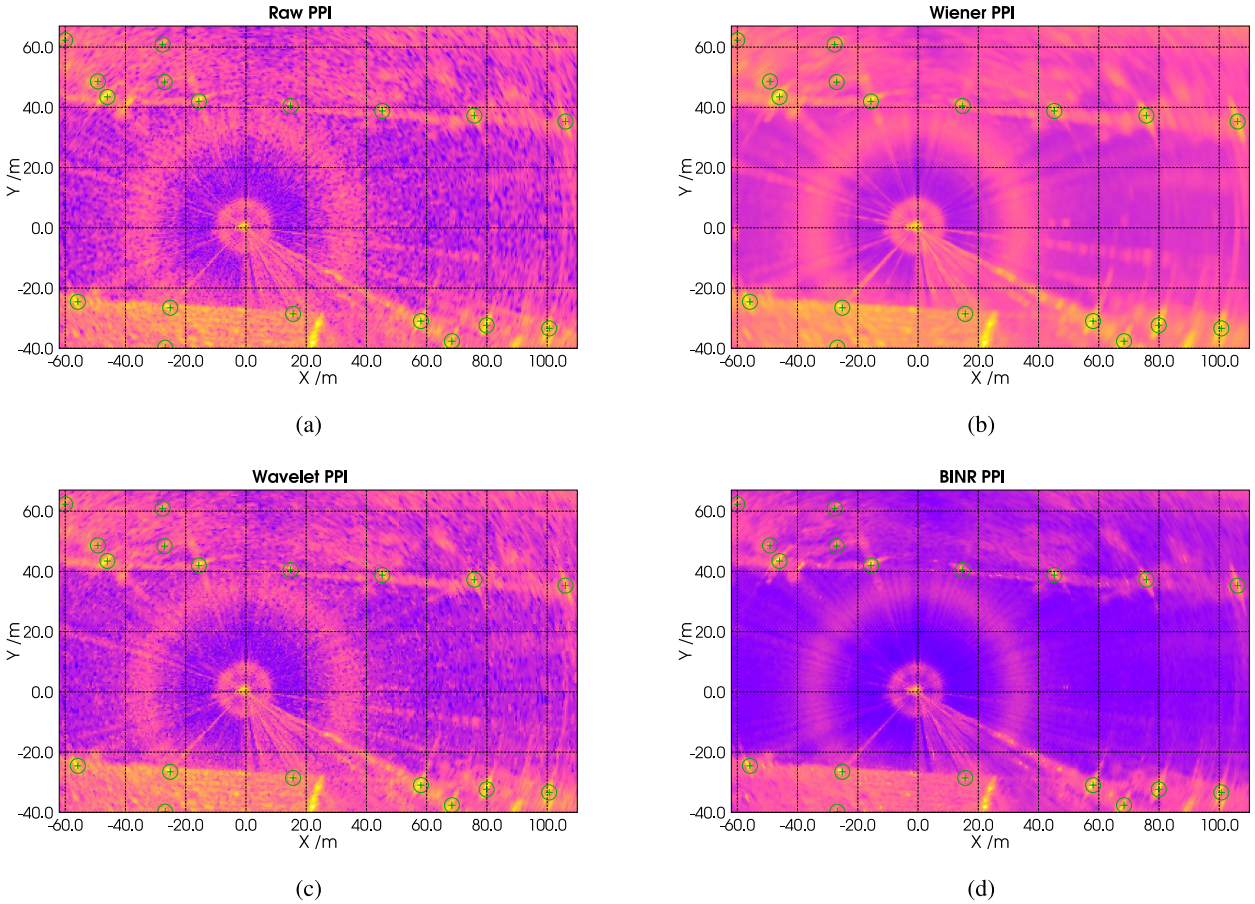

Fig. 5. Raw power and reduced noise power PPI plots of the park area. (a) PPI showing noisy input data from the park environment. (b) PPI showing Wiener filtered data from the park environment. (c) PPI showing Wavelet denoised data from the park environment. (d) PPI showing BINR data from the park environment.

The Wiener support region was 3 bins in the range and bearing direction, which is the expected power spread of the targets of interest.

In the case of the spatial (2D) wavelet denoising, the Daubechies 3 wavelet function was used, while the Haar wavelet was selected for the 1D (temporal) dimension.

The noisy raw radar input data from the park is presented in Figure 5a. The ground truth location of lamp posts and trees are marked with green circles and a cross in their centre.

Wiener filtering (Figure 5b) exhibits a smoother noise background but the main objects identified in the scene are blurred by the filter, thus losing localisation detail. Wavelet denoising (Figure 5c), is able to preserve the location and edges of targets. It does, however, produce several negative values in noise only sections, which are truncated to a small value to allow visualisation. Nevertheless, the average noise level is reduced. Finally, the BINR method in Figure 5d shows its ability to retain details as well as to reduce the noise level. It can, however, be observed that some of the maximum power peaks have been reduced in magnitude (e.g. tree at $(-49.1$ m, 48.6 m); with a raw power value of 86.02 dB and a BINR power value of 82.73 dB). This is due to the fact that at some observation l those particular targets were not detected, therefore their power values were considered noise and thus subtracted from them. Note that wavelet denoising (Figure 5c) reduces some noise-only areas to very low values. However, the noise background is not homogeneous, therefore, the sharp edges between noise areas near the average noise level and those greatly reduced by the wavelet method can yield several false detections as will be shown, after applying the CA-CFAR detector.

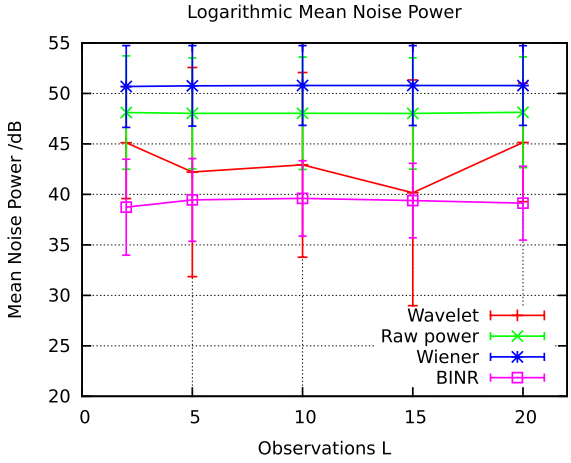

Fig. 6. Noise mean values and variances from a noise only area.

Figure 6 shows mean noise power values from each method, in an area which is known to contain no targets. The BINR

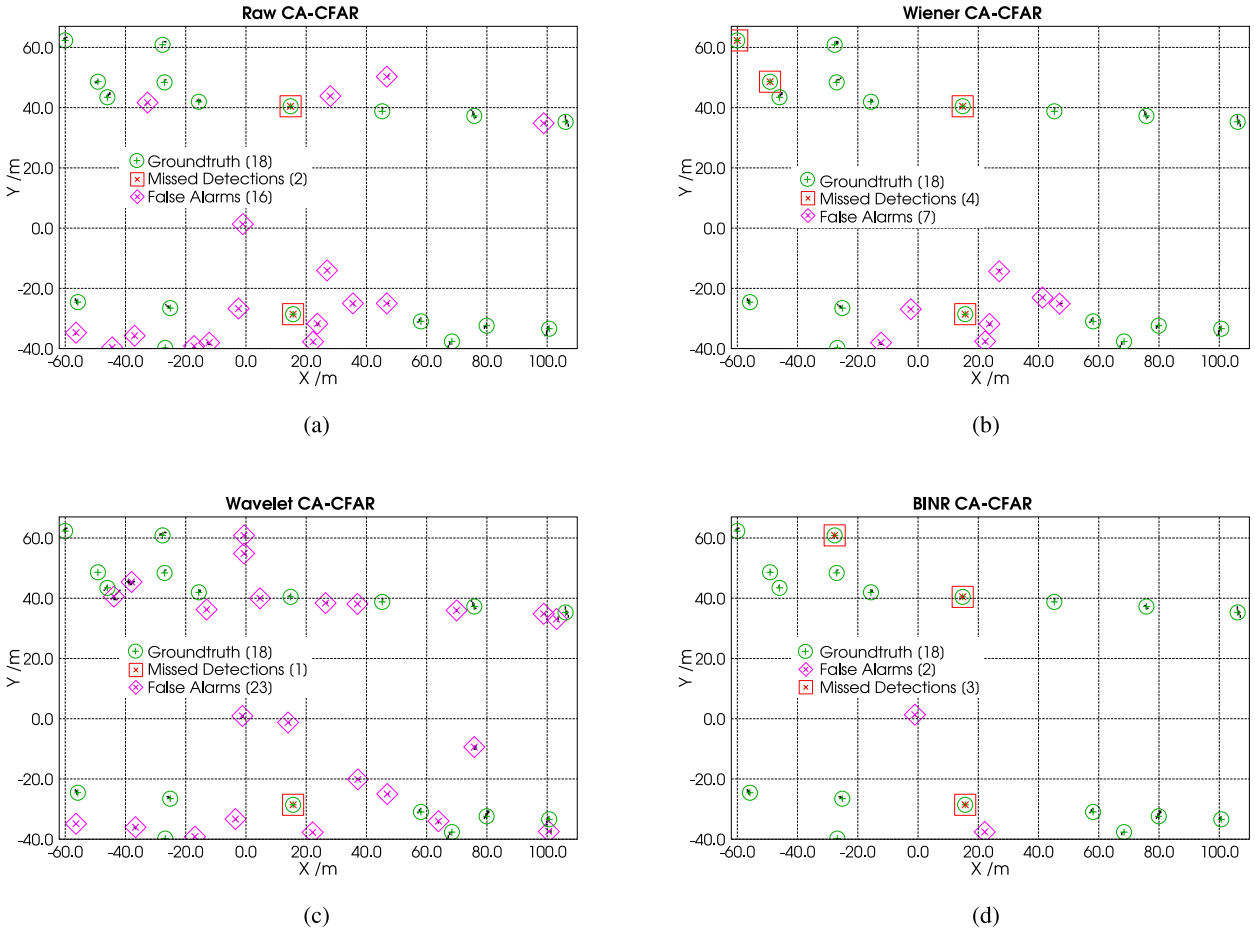

Fig. 7. CA-CFAR detector applied to raw and reduced noise power in the park area. (a) CA-CFAR PPI showing noisy input data from park environment. (b) CA-CFAR PPI showing Wiener filtered data from park environment. (c) CA-CFAR PPI showing Wavelet denoised data from park environment. (d) CA-CFAR PPI showing BINR data from the park environment.

method exhibits the the lowest mean noise power for all L values. Its variance, on the other hand, is higher than that of the Wiener for small L values, but as more observations are included, BINR achieves also the lowest noise variance. The Wiener filter mean noise power stays above that of the raw data, but keeps the variance at a low value. The Wavelet denoising method is able to reduce the mean noise power lower than the raw data but is not able to reach the value of the BINR method. The Wavelet's variance remains high and oscillates due to the ripple effect mentioned before. The noise assumptions which form the basis of all three noise reduction techniques are violated in practice. In particular, the Wiener filter is not optimal for non-Gaussian noise distributions. In the case of the wavelet method, the universal threshold is not able to correctly estimate a noise threshold to separate the noise and information based wavelet coefficients. Furthermore, noise information is no longer spread homogeneously across all wavelet coefficients. Likewise, the CFAR method used in the BINR yields a higher false alarm rate than expected, since exponential noise is assumed, as will be shown in the next section.

2) Target Detection: The CA-CFAR detector is applied to the reduced noise data, in order to demonstrate the usefulness of each noise reduction method. In this case a more relaxed CA-CFAR probability of false alarm is applied ($P_{fa} = 1 \times 10^{-3}$), which reduces $\tau^{\text{CA-CFAR}}$ and increments the $P_D^{\text{CA-CFAR}}$ (see Equations (1) and (2)). This is possible since the reduced noise data is expected to yield a lower false alarm rate, and it helps to overcome the lower target power values obtained in all three methods due to smoothing, thresholding or noise subtraction.

Figure 7a shows the result of the detector applied to the raw noisy input data. The detector itself is able to reduce false alarms to some extent in the raw data. Again, the green circles in the figure denote the ground truth location of some relevant targets (trees and lamp posts at the side of the track) obtained using multiple scans from a laser scanner. CA-CFAR detections are marked with black dots, when these dots are in the vicinity of a ground truth marker, they are considered correct detections. Red square markers are used to show missed detections, while magenta coloured diamonds are used to mark false alarms. The Wiener filter (Figure 7b), interestingly, shows a remarkable reduction of background noise, but its blurring effects present some problems. In particular, small and medium size targets with low SNP are blurred in such a way that their size is reduced and even completely removed from the CA-CFAR detector output. On the other hand, high SNP targets become increased in size (more pixels surrounding

TABLE II
A POSTERIORI DETECTION AND FALSE ALARM RATES

Method	T_D	T_G	T_{fa}	T_N	R_D	R_{fa} /10^{-3}
Raw	16	18	23	81919	0.89	0.2807
Wiener	14	18	14	81943	0.78	0.1708
Wavelet	17	18	88	81712	0.94	1.0758
BINR	15	18	2	81977	0.83	0.0244

TABLE III
OSPA METRIC APPLIED TO EACH METHOD

L	Raw power	Wiener	Wavelet	BINR
2	1.6747	1.6225	1.6565	1.5401
5	1.7055	1.6174	1.8435	1.5230
10	1.6770	1.6377	1.7328	1.4486
15	1.7013	1.6230	1.8673	1.4365
20	1.6796	1.6025	1.7878	1.5114

the landmark are marked as detections), for instance, the tree at coordinates (−27.0 m, 48.4 m). In general, edge details are lost. Figure 7c presents the results of applying the detector to the wavelet denoised data. The method, is able to keep feature details but it shows more false alarms than expected, especially in broad "noise-only" areas. This is due to the noise background not being homogeneous, which leads to the ripple effect of the chosen wavelet function, and the universal threshold not being able to correctly discriminate between information and noise wavelet coefficients. The BINR method (Figure 7d), is able to preserve localisation details, e.g. targets at (−25.1 m, −26.6 m), (68.4 m, −37.6 m) and (100.7 m, −33.4 m), as well as reduce the number of false alarms when compared to the detector applied to raw data and the other noise reduction methods.

A posteriori detection and false alarm rates can be derived from the results. Detection rate, R_D, is obtained by dividing the number of correctly detected ground truth targets, T_D, and the total number of ground truth targets, T_G, i.e. $R_D = T_d/T_G$. The False alarm rate, R_{fa}, on the other hand, is calculated by dividing the number of pixels corresponding to false alarms, T_{fa}, and the sum of pixels correctly identified as noise, T_N, plus the false alarm pixels, i.e. $R_{fa} = T_{fa}/(T_{fa} + T_N)$. Table II summarises the detection and false alarm rates calculation. Note that the area, where the experiment was carried out, exhibits a lower false alarm rate than expected (0.281×10^{-3}), with a detection rate of 89%. The Wiener filter yields a lower false alarm rate (0.171×10^{-3}) but in the same order of magnitude. The detection rate is also lower (78%) than in the raw image. Wavelet denoising's detection rate is higher (94%), but its false alarm rate is higher by an order of magnitude (1.076×10^{-3}). BINR is able to reduce the false alarm rate by an order of magnitude (0.024×10^{-3}), with a detection rate (83%) higher than the Wiener filter, but lower than the raw data. From this result, it can be seen that using BINR it is safe to increase the $P_{fa}^{\text{CA-CFAR}}$ value in order to get a higher detection rate while still achieving a low false alarm rate.

3) Quantifying Detection Performance: While there are several metrics to quantify the error between detected and true targets, a metric is now applied (which jointly considers errors in target location, and number estimates), based on a p^{th} order Wasserstein construction [30]. This metric has been recently introduced and has been shown to produce more consistent results than others (Hausdorff, OMAT) in multi-object systems. It is formulated in terms of the ground truth set of targets $\widehat{\mathcal{M}}$ and the detected set $\mathcal{M}$. If $|\mathcal{M}| > |\widehat{\mathcal{M}}|$, it is given by,

$$\bar{d}^{(\upsilon)}(\widehat{\mathcal{M}}, \mathcal{M}) = \left(\frac{1}{|\mathcal{M}|}\left(\min_{\pi \in \Pi_k} \sum_{i=1}^{|\widehat{\mathcal{M}}|} d^{(\upsilon)}\left(\widehat{m}^i, m^{\pi(i)}\right)^p + \upsilon^p\left(|\mathcal{M}| - |\widehat{\mathcal{M}}|\right)\right)\right)^{1/p} \tag{14}$$

where π corresponds to the permutation in Π_k (the set of permutations on $\{1, 2, \ldots, k\}$) which minimises the sum of the distances between the elements from $\widehat{\mathcal{M}}$ and $\mathcal{M}$, while

$$d^{(\upsilon)}(\widehat{m}^i, m^{\pi(i)}) = \min(\upsilon, ||\widehat{m}^i - m^{\pi(i)}||) \tag{15}$$

is the minimum of the cut-off parameter, υ, and the Euclidean distance between the ground truth target location, $\widehat{m}^i$ and the detected target location $m^{\pi(i)}$. If $|\mathcal{M}| < |\widehat{\mathcal{M}}|$ the metric is obtained through $\bar{d}^{(\upsilon)}(\mathcal{M}, \widehat{\mathcal{M}})$. To find the optimal $\pi \in \Pi_k$ a special case of integer linear programming is required, which can be solved efficiently using the Hungarian method for optimal point assignment.

This metric was applied to the CA-CFAR output of the reduced noise images to quantify the performance of each method. The results for different L values are shown in Table III. Because of the range and angular resolution of the radar used in this experiment, for each ground truth landmark, more than one point is marked as a detection. This increases the error measured by the metric because extra points are considered as false alarms. Thus, the metric output starts to converge to the cut-off parameter, as the second term to the right of Equation (14) dominates. A method to reduce this effect is to combine multiple detections in close proximity using a clustering method, e.g. *connected component labelling* [32]. A different approach, consisting of duplicating the elements of the ground truth set, was used in this implementation, which effectively reduces the effect described above, without altering the results. For all L values, the BINR methods yields a smaller value of the metric meaning that the produced map is closer to the ground truth than that generated by the raw data and the other methods. The Wiener filter is also capable of producing a map with a lower error than the raw data. On the other hand, the Wavelet denoising shows a poor performance due to the false alarms in the background noise caused by the ripple effect within the Wavelet transform.

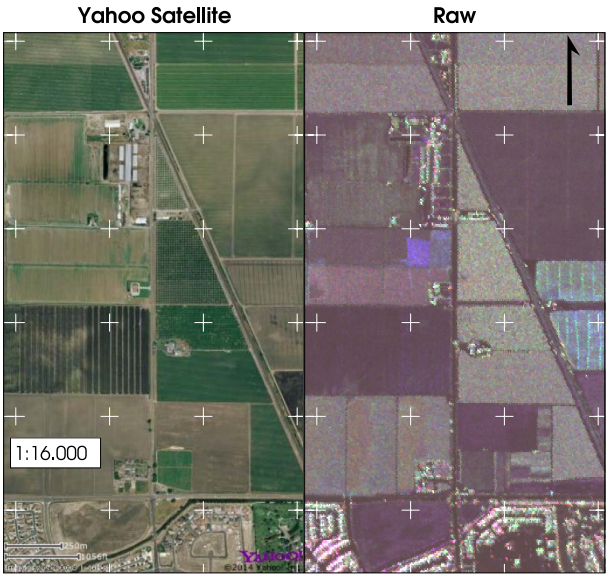

Fig. 8. Yahoo Satellite view (left) and Raw SAR image of the area (right).

C. UAVSAR Data Set

Detection and noise reduction methods in radar are not only used in classical A-Scopes, B-Scopes and PPIs, they can also be used in other forms of radar data such as SAR images [20], [33].

SAR images, being constructed in a fundamentally different way than the classical radar images, are also affected by noise in a different way. In SAR images, noise and clutter are usually modelled by a Weibull or K distribution. Also, the effect of multiplicative speckle noise in SAR images is higher than in other forms of radar data. Under these conditions, the Ordered Statistics (OS) CFAR detection method has proven to be effective when applied to SAR images [34].

In this section the results of using the BINR method on a set of SAR images obtained from the NASA Jet Propulsion Lab (JPL)'s Uninhabited Aerial Vehicle SAR (UAVSAR) mission[5] are presented.

The images correspond to a location near Sacramento, CA, which covers an area of crop fields with isolated buildings in the north-most part (top) of the image and a suburban area with high density housing in the south-most part (bottom). Figure 8 (left) shows a Yahoo Satellite image of the area, with its corresponding SAR image (right). The area is 1.6 km in the horizontal (east-west) direction and 2.88 km in the vertical (north-south) direction. These SAR images represent backscatterred radar power, polarised in the HH, HV and VV components. The magnitude of each component is encoded in the image's red, green and blue channels, respectively.

BINR based on the OS-CFAR detector has been used to first reduce the noise in a series of multiple ($L = 6, M^{\mathrm{BI}} = 3$) observations of the same area. Then the OS-CFAR detector is applied to the reduced noise data to detect buildings. The OS-CFAR window size was 7 bins in the x and y coordinates, while the guard cells window size was 3 bins in both directions. The threshold's constant parameter chosen was $\tau^{\text{OS-CFAR}} = 4.16707$, this value is obtained by solving Eq. (6) using the OS-CFAR window size and the desired value for $P_{fa}^{\text{OS-CFAR}}$. Finally, the noise subtraction parameters used were $\alpha_d = 0.9$, $c = 50.0$ and $d = 0.1$.

[5]UAVSAR data courtesy NASA/JPL-Caltech. http://uavsar.jpl.nasa.gov/

TABLE IV
MEAN NOISE POWER AND VARIANCE IN NOISE ONLY AREA IN dB

	HH		HV		VV	
Method	Mean	Var.	Mean	Var.	Mean	Var.
Raw	24.96	160.85	29.14	350.91	28.62	169.56
Wiener	27.58	159.20	36.59	437.78	32.74	180.68
Wavelet	-13.64	1434.88	-9.62	916.63	-9.75	1042.87
BINR	14.38	166.84	20.30	383.10	19.26	204.06

The parameters for Wavelet denoising and Wiener filtering were the same as those used in the experimental data set presented in Section V-B.

All three polarisation components have been processed. Buildings, in general, reflect radar waves similarly in all polarisations while vegetation and other terrain considered to be clutter in this case, usually exhibit different back-scatter intensity at the different polarisations. The raw power (left) and the output of the OS-CFAR detector are shown in Figure 9a. In the OS-CFAR image, the red, green and blue pixels corresponds to detections in the HH, HV and VV polarisations, respectively. Cyan, magenta and yellow pixels represent detections in the respective combinations of two polarisations, while white pixels represent detections in all three polarisations. Buildings appear in the OS-CFAR image with white pixels (detections in all polarisations), while parks and crop fields present detections in single polarisations or no detection at all.

The Wiener filtering results are presented in Figure 9b. The reduced noise image appears blurred, as expected from the Wiener filter, and the OS-CFAR detector is unable to detect buildings from the crop fields.

The wavelet denoising output is shown in Figure 9c. The power image shows darker colours meaning that the average noise power has been reduced, but several areas present a high variance, particularly in the crop fields. The OS-CFAR output confirms this, and the detector is unable to detect building structures.

Figure 9d corresponds to BINR output. It can be observed that the areas corresponding to crop fields appear smoothed when compared to the raw image. It can also be observed that the number of detections in single polarisations, mostly located in areas corresponding to crop fields, is reduced in the BINR image. On the other hand, most pixels corresponding to building like structures are preserved.

In this data set it is not possible to apply the OSPA metric as the real ground truth is unavailable. An analysis on the noise statistics in an area with no targets, as was carried out in the park data set, quantifies the performance of the noise reduction methods. Table IV shows the mean noise power and variance per polarisation channel. It can be observed that the

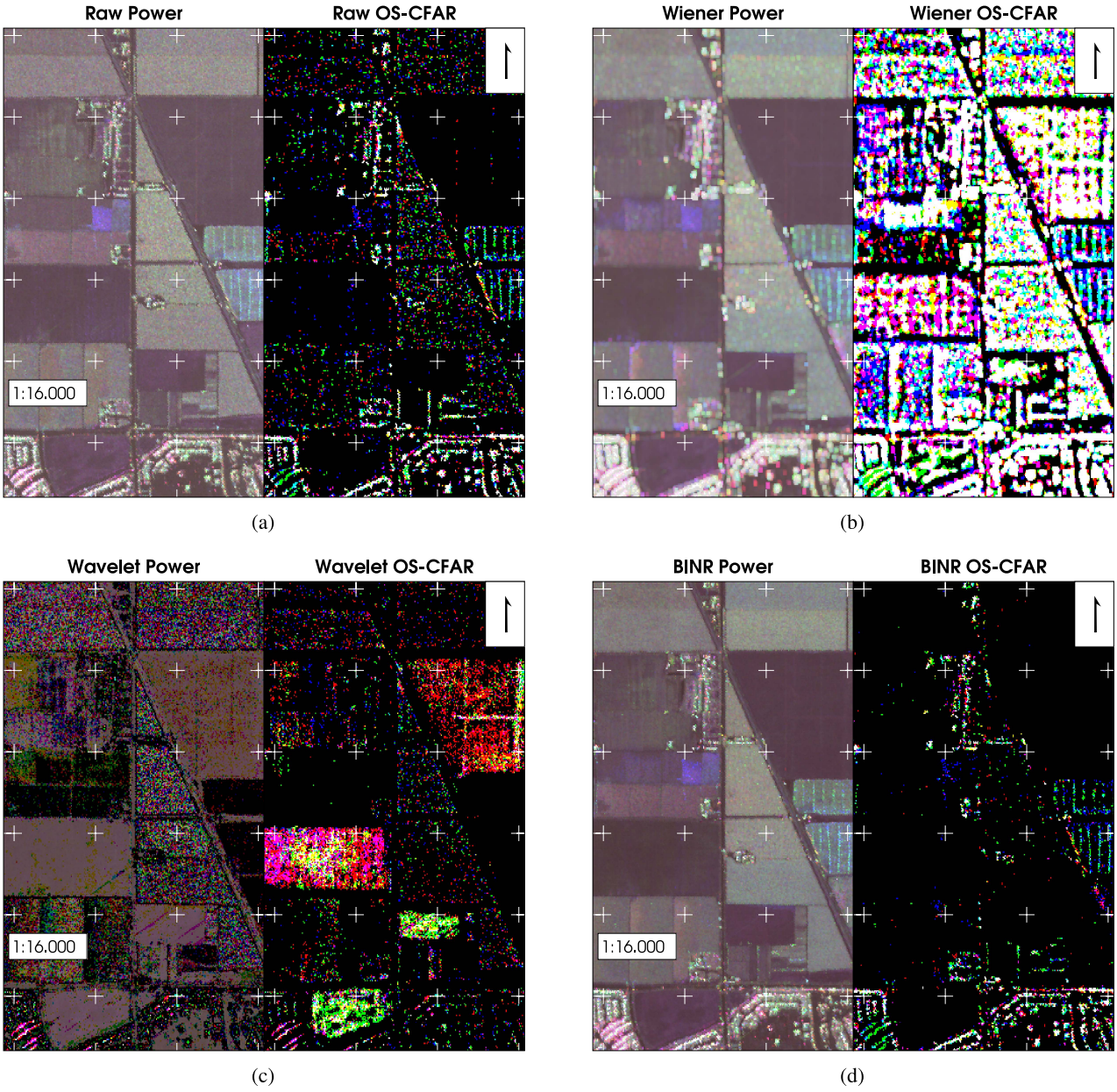

Fig. 9. Raw and reduced noise power SAR images and OS-CFAR applied to them. (a) Raw power SAR image (left) and OS-CFAR applied to it (right). (b) Wiener reduced noise SAR image (left) and OS-CFAR applied to it (right). (c) Wavelet reduced noise SAR image (left) and OS-CFAR applied to it (right). (d) BINR SAR image and OS-CFAR applied to it.

Wavelet presents the lowest mean noise power, but at the same time it yields a very high variance. The Wiener and BINR methods keep a variance similar to that of the original data, but BINR is able to reduce the mean noise level considerably, while the Wiener filter noise level stays at a similar or higher value than the raw data.

VI. Conclusion

In this work, a noise reduction method based on the binary integrator detector and spectral noise subtraction has been introduced. Its performance has been compared with two other general, widely used, noise reduction methods, Wiener filtering and wavelet denoising.

As detailed in Section V, the BINR method exhibits good noise reduction capabilities, which result in a higher signal-to-noise power ratio than the other two techniques. Importantly, BINR has the ability to preserve most of the signal's spatial details. Also, the BINR algorithm's computational time is lower than the other two methods. The reduced time complexity shown by the BINR method and its denoising capabilities make it an appealing noise reduction alternative to be used as a pre-processing step for radar data.

The encouraging results obtained open the door for several improvements for radar data noise reduction. One track for improvement lies in enhancing the standard Wiener or Wavelet methods by making them adaptable to different noise distributions. This approach has been adopted for some

wavelet denoising applications in which different threshold functions are derived for some non-Gaussian noise distributions [12], [35], [36]. This can then be the basis for the integration of 2 or more of the methods. This has been carried out for Wiener and Wavelet filtering in the work of Jin et al. [13]. This work exploited the advantages of both methods simultaneously, but even though the theoretical improvement in peak-to-peak SNR was expected to be 3dB, only 0.5dB was achieved. Also the time complexity of Jin et al's method corresponds to the combination of both the Wiener and wavelet methods. In particular, it would be interesting to evaluate optimised combinations of the Wiener filter and BINR, Wavelet denoising and BINR, and the Wiener-Wavelet and the BINR method, in terms of their computational complexities. These combinations would be expected to yield the advantages of the individual methods, for instance, the smooth background noise presented by the Wiener filter, the reduction in the mean noise power value provided by the BINR method, and the faithful representation of the original signal achieved when applying wavelet denoising.

ACKNOWLEDGMENT

The authors would like to thank NASA/JPL-Caltech for all UAVSAR data.

REFERENCES

[1] J. C. Brailean, R. P. Kleihorst, S. Efstratiadis, A. K. Katsaggelos, and R. L. Lagendijk, "Noise reduction filters for dynamic image sequences: A review," *Proc. IEEE*, vol. 83, no. 9, pp. 1272–1292, Sep. 1995.

[2] N. Wiener, *Extrapolation, Interpolation, and Smoothing of Stationary Time Series*. Cambridge, MA, USA: MIT Press, 1964.

[3] B. Widrow *et al.*, "Adaptive noise cancelling: Principles and applications," *Proc. IEEE*, vol. 63, no. 12, pp. 1692–1716, Dec. 1975.

[4] M. Martin-Fernandez, C. Alberola-Lopez, J. Ruiz-Alzola, and C.-F. Westin, "Sequential anisotropic Wiener filtering applied to 3D MRI data," *Magn. Reson. Imag.*, vol. 25, no. 2, pp. 278–292, 2007. [Online]. Available: http://www.sciencedirect.com/science/article/pii/S0730725X06002852

[5] I. N. Daliakopoulos and I. K. Tsanis, "A weather radar data processing module for storm analysis," *J. Hydroinformat.*, vol. 14, no. 2, pp. 332–344, 2012.

[6] D. Donoho, "De-noising by soft-thresholding," *IEEE Trans. Inf. Theory*, vol. 41, no. 3, pp. 613–627, May 1995.

[7] D. L. Donoho and J. M. Johnstone, "Ideal spatial adaptation by wavelet shrinkage," *Biometrika*, vol. 81, no. 3, pp. 425–455, 1994. [Online]. Available: http://biomet.oxfordjournals.org/content/81/3/425.abstract

[8] D. L. Donoho and I. M. Johnstone, "Threshold selection for wavelet shrinkage of noisy data," in *Proc. 16th Annu. Int. Conf. IEEE Eng. Med. Biol. Soc. Eng. Adv., New Opportunities Biomed. Eng.*, vol. 1. no. 12, Nov. 1994, pp. A24–A25.

[9] C. Burrus, R. Gopinath, and H. Guo, *Introduction to Wavelets and Wavelet Transforms: A Primer*, vol. 23. Upper Saddle River, NJ, USA: Prentice-Hall, 1998.

[10] M.-Y. Chen and J.-J. Chao, "Radar image denoising by recursive thresholding," in *Proc. Int. Conf. Image Process.*, vol. 1. Sep. 1996, pp. 395–398.

[11] O. A. M. Aly, A. S. Omar, and A. Z. Elsherbeni, "Detection and localization of RF radar pulses in noise environments using wavelet packet transform and higher order statistics," *Prog. Electromagn. Res.*, vol. 58, pp. 301–317, 2006. [Online]. Available: http://jpier.org/pier/pier.php?paper=0507024

[12] Y. Chen and C. Han, "Adaptive wavelet thresholding for image denoising and compression," *Electron. Lett.*, vol. 41, no. 10, pp. 586–587, May 2005.

[13] F. Jin, P. Fieguth, L. Winger, and E. Jernigan, "Adaptive wiener filtering of noisy images and image sequences," in *Proc. Int. Conf. Image Process. (ICIP)*, vol. 3. Sep. 2003, pp. III-349–III-352.

[14] S. Boll, "Suppression of acoustic noise in speech using spectral subtraction," *IEEE Trans. Acoust., Speech, Signal Process.*, vol. 27, no. 2, pp. 113–120, Apr. 1979.

[15] M. I. Skolnik, Ed., "Automatic detection, tracking, and sensor integration," in *Radar Handbook*, 3rd ed. New York, NY, USA: McGraw-Hill, 2008.

[16] P. P. Gandhi and S. A. Kassam, "Optimality of the cell averaging CFAR detector," *IEEE Trans. Inf. Theory*, vol. 40, no. 4, pp. 1226–1228, Jul. 1994.

[17] A. Foessel, J. Bares, and W. R. L. Whittaker, "Three-dimensional map building with MMW radar," in *Proc. 3rd Int. Conf. Field Service Robot.*, Helsinki, Finland, Jun. 2001. [Online]. Available: http://www.ri.cmu.edu/publication_view.html?pub_id=3758&menu_code=0307

[18] D. Langer, "An integrated MMW radar system for outdoor navigation," in *Proc. IEEE Int. Conf. Robot. Autom.*, Minneapolis, MN, USA, Apr. 1996, pp. 417–422.

[19] M. Barkat, *Signal Detection and Estimation,* ser. Artech House Radar Library. Norwood, MA, USA: Artech House, 2005. [Online]. Available: http://books.google.com/books?id=Le5SAAAAMAAJ

[20] G. Gao, L. Liu, L. Zhao, G. Shi, and G. Kuang, "An adaptive and fast CFAR algorithm based on automatic censoring for target detection in high-resolution SAR images," *IEEE Trans. Geosci. Remote Sens.*, vol. 47, no. 6, pp. 1685–1697, Jun. 2009.

[21] H. Rohling, "Radar CFAR thresholding in clutter and multiple target situations," *IEEE Trans. Aerosp. Electron. Syst.*, vol. AES-19, no. 4, pp. 608–621, Jul. 1983.

[22] N. Wiener, *Extrapolation, Interpolation, and Smoothing of Stationary Time Series: With Engineering Applications* (Technology Press Books in Science and Engineering). Cambridge, MA, USA: MIT Press, 1949.

[23] A. Kolmogorov, *Stationary Sequences in Hilbert Space*. Chicago, IL, USA: John Crerar Library, 1978.

[24] J.-S. Lee, "Digital image enhancement and noise filtering by use of local statistics," *IEEE Trans. Pattern Anal. Mach. Intell.*, vol. PAMI-2, no. 2, pp. 165–168, Mar. 1980.

[25] D. L. Donoho and I. M. Johnstone, "Ideal denoising in an orthonormal basis chosen from a library of bases," *Comptes Rendus Acad. Sci., Ser. I*, vol. 319, no. 12, pp. 1317–1322, 1994.

[26] G. Luo and D. Zhang, "Wavelet denoising," in *Advances in Wavelet Theory and Their Applications in Engineering, Physics and Technology*. Rijeka, Croatia: InTech, 2012, pp. 59–80. [Online]. Available: http://www.intechopen.com/

[27] I. Cohen and B. Berdugo, "Noise estimation by minima controlled recursive averaging for robust speech enhancement," *IEEE Signal Process. Lett.*, vol. 9, no. 1, pp. 12–15, Jan. 2002.

[28] M. Berouti, R. Schwartz, and J. Makhoul, "Enhancement of speech corrupted by acoustic noise," in *Proc. IEEE Int. Conf. Acoust., Speech, Signal Process. (ICASSP)*, vol. 4. Apr. 1979, pp. 208–211.

[29] E. Jones, T. Oliphant, and P. Peterson. (2001). *SciPy: Open Source Scientific Tools for Python*. [Online]. Available: http://www.scipy.org/

[30] S. Kuttikkad and R. Chellappa, "Non-Gaussian CFAR techniques for target detection in high resolution SAR images," in *Proc. IEEE Int. Conf. Image Process. (ICIP)*, vol. 1. Nov. 1994, pp. 910–914.

[31] E. Widzyk-Capehart, G. Brooker, S. Scheding, R. Hennessy, A. Maclean, and C. Lobsey, "Application of millimetre wave radar sensor to environment mapping in surface mining," in *Proc. 9th Int. Conf. Control, Autom., Robot. Vis. (ICARCV)*, Dec. 2006, pp. 1–6.

[32] D. Schuhmacher, B.-T. Vo, and B.-N. Vo, "A consistent metric for performance evaluation of multi-object filters," *IEEE Trans. Signal Process.*, vol. 56, no. 8, pp. 3447–3457, Aug. 2008.

[33] L. Shapiro and G. Sockman, *Computer Vision*. Englewood Cliffs, NJ, USA: Prentice-Hall, 2002, ch. 3.

[34] M. di Bisceglie and C. Galdi, "CFAR detection of extended objects in high-resolution SAR images," in *Proc. IEEE Int. Geosci. Remote Sens. Symp. (IGARSS)*, vol. 6. Jul. 2001, pp. 2674–2676.

[35] S. Zhong and V. Cherkassky, "Image denoising using wavelet thresholding and model selection," in *Proc. Int. Conf. Image Process.*, vol. 3. 2000, pp. 262–265.

[36] A. Antoniadis, D. Leporini, and J.-C. Pesquet, "Wavelet thresholding for some classes of non–Gaussian noise," *Statist. Neerlandica*, vol. 56, no. 4, pp. 434–453, 2002.

Daniel Lühr (S'99–M'04) was born in Santiago, Chile, in 1978. He received the Lic.Sci. and Diploma degrees in electrical engineering from the University of Chile, Santiago, Chile, in 2003 and 2004, respectively.

He was a Research Associate and No-Fee Consultant with the Submillimeter Receiver Laboratory, Harvard-Smithsonian Center for Astrophysics, Cambridge, MA, USA, from 2004 to 2006. From 2007 to 2009, he was an Adjunct Professor with the Universidad Austral de Chile, Valdivia, Chile. From 2009 to 2013, he was a Consultant with the Chilean Ministry of Energy. He is currently with the Department of Electrical Engineering, University of Chile. He has expertise in digital systems, system integration, medical devices, and robotics. His current research interests include robotics and its applications.

Martin Adams (SM'08) received the degree in engineering science from the University of Oxford, Oxford, U.K., in 1988, and the Ph.D. degree from the Robotics Research Group, University of Oxford, in 1992. He is currently a Professor of Electrical Engineering with the Department of Electrical Engineering, University of Chile, Santiago, Chile. He is also a Principle Investigator with the industrially sponsored Advanced Mining Technology Centre, University of Chile. After his Ph.D., he continued his research in autonomous robot navigation as a Project Leader and part-time Lecturer with the Institute of Robotics, Swiss Federal Institute of Technology, Zurich, Switzerland. He was a Guest Professor and taught control theory in St. Gallen, Switzerland, from 1994 to 1995. From 1996 to 2000, he served as a Senior Research Scientist in Robotics and Control, in the field of semiconductor assembly automation, with the European Semiconductor Equipment Centre, Cham, Switzerland. From 2000 to 2010, he was an Associate Professor with the School of Electrical and Electronic Engineering, Nanyang Technological University, Singapore. His research work focuses on autonomous robot navigation, sensing, and multiobject estimation, and has authored many technical papers in these fields. He has been a Principle Investigator and leader of many robotics projects, coordinating researchers from local industries and local and overseas universities, and has served as an Associate Editor of various journal and conference editorial boards.